Available online at www.sciencedirect.com
ScienceDirect
Coastal Engineering 53 (2006) 983–996
Coastal Engineering
An International Journal for Coastal, Harbour and Offshore Engineers
www.elsevier.com/locate/coastaleng

Bed load transport on the shoreface by currents and waves

Maarten G. Kleinhans *, Bart T. Grasmeijer

Institute for Marine and Atmospheric Research, Department of Physical Geography, Utrecht University, PO-Box 80115, 3508 TC Utrecht, The Netherlands

Received 22 November 2005; received in revised form 22 February 2006; accepted 13 June 2006
Available online 9 August 2006

Abstract

Tide-driven bed load transport is an important portion of the net annual sediment transport rate in many shoreface and shelf environments. However, bed load transport under waves cannot be measured in the field and bed load transport by currents without waves is barely measurable, even in spring tidal conditions. There is, consequently, a strong lack of field data and validated models. The present field site was on the shoreface and inner shelf at 2 to 8.5 km offshore the central Dutch coast (far outside the surfzone), where tidal currents flow parallel to the coast. Bed load transports were carefully measured with a calibrated sampler in spring tidal conditions without waves at a water depth of 13–18 m with fine and medium sands. The near-bed flow was measured over nearly a year and used for integration to annual transport rates. An empirical bed load model was derived, which predicts bed load transports that are a factor of >5 smaller than predicted by existing models. However, they agree with laboratory data of sand and gravel transport in currents near incipient motion. The damped transport rates may have been caused by cohesion of sediment or turbulence damping due to mud or biological activity. The annual bed load transport rate was calculated using a probability density function (pdf) derived from the near-bed current and orbital velocity data which represented the current and wave climate well when compared to 30 years of data from a nearby wave station. The effect of wave stirring was included in the transport calculations. The net bed load transport rate is a few m^2/year. This is much less than predicted in an earlier model study, which is partly due to different bed load models but also due to the difference in velocity pdf. The annual transport rate is very sensitive to the probability of the largest current velocities.

Keywords: Shoreface; Continental shelf; Ocean waves (sediment transport); Bed load transport; Field measurements; Wave climate; Current climate; Bed load sampling

1. Introduction

A better understanding is needed of the sediment dynamics on the shoreface and shelf for sand mining and long-term coastal development purposes (Van Rijn et al., 2005a). So far, only model output and trench filling data is available as an estimate of sediment transport (Van Rijn, 1997), which has been used widely for research and coastal management work. Bed load models are mostly calibrated on laboratory data or data collected in rivers (Ribberink, 1998; Soulsby and Damgaard, 2005). The model study of Van Rijn (1997) indicated that the bed load transport rate was equal to the suspended load transport at water depths of 8–20 m, which underscores the importance of bed load transport in shelf environments and the pressing need for field data of bed load transport. The field measurements presented in this paper now allow for model testing.

An important part of the total sediment transport is driven by tidal currents combined with stirring by waves. In current dominated conditions in many shelf environments, the bed shear stress is near the critical Shields parameter for incipient motion for a large proportion of the tidal cycle. Unfortunately, bed load transport under waves cannot be measured in the field and bed load transport by currents without waves is difficult to measure, even in spring tidal conditions with relatively strong currents. There is, consequently, a strong lack of field data and validated models. Conversely, bed load transport in tidal currents may be measurable with samplers. Moreover, bed load predictors for currents can also be applied to conditions with waves or waves plus currents (Madsen and Grant, 1976; Ribberink, 1998; Soulsby and Damgaard, 2005). This means that an empirical bed load predictor based on measurements in tidal current conditions without waves can potentially be

* Corresponding author.
E-mail addresses: m.kleinhans@geo.uu.nl (M.G. Kleinhans), b.grasmeijer@geo.uu.nl (B.T. Grasmeijer).
URL's: http://www.geog.uu.nl/fg/mkleinhans (M.G. Kleinhans), http://www.coastalresearch.nl (B.T. Grasmeijer).

0378-3839/$ - see front matter © 2006 Elsevier B.V. All rights reserved.
doi:10.1016/j.coastaleng.2006.06.009

applied to conditions with waves. This will be the approach in this paper. Suspended transport and annual total transport is covered in a forthcoming contribution and in Grasmeijer et al. (2005).

The objectives of this paper are: (1) to present the bed load measurements in tidal conditions, (2) to scale these up to the annual gross and net bed load transport rates on the shoreface and shelf along the Dutch coast, and (3) to test the sensitivity of the upscaling to the sediment transport predictor and the representation of the current and wave climate. First, the field site and measurement methodology are introduced. Next, the calculation methods of shear stress and sediment transport are given. The results of the measurements and calculations are given in Section 3. The discussion (Section 4) focuses on the importance of the criterion for initial motion and the potential effects of mud or biotic cohesion in the bed, on the comparison of the bed load predictors and, finally, on the representation of the wave and current climate on the annual transport rates.

2. Field site and methodology

2.1. Measurements

The field sites are located on the central Dutch shoreface and shelf in the North Sea, 2 and 8.5 km off Noordwijk at an average water depth of 13 and 18 m (Fig. 1. The bed load data of Van de Meene and Van Rijn (2000) off the coast of Zandvoort are used as part of the present data in the whole analysis since they were collected in the same area with the same measurement method (Table 1). All sites are far offshore from the surfzone. The tidal currents are semi-diurnal and are directed parallel to the coast. The spring tidal amplitude is 1.3 m and maximum depth-averaged tidal currents are between 0.4 and 0.8 m/s. The incident wave angle during storms varies between 50 and 130° (North=0°) or −40 to 40° (cross-shore=0°). In storms the H_{m0} wave height at 13 m water depth may become larger than 4 m. The bed sediment is fine to medium sand, fining up the shoreface (Table 1).

Table 1
Bed load sampling campaigns and sites

Date	Site	Depth (m)	Offshore (km)	Location	D_{10} (mm)	D_{50} (mm)	D_{90} (mm)
14 August 1991	Zandvoort	14	7.3	Top ridge	0.244	0.280	0.336
5 March 2003	Noordwijk	13	2.2	Shoreface	0.160	0.216	0.288
25 Sept 2003	Noordwijk	13	2.2	Shoreface	0.185	0.227	0.305
6 Nov 2003	Noordwijk	18	8.5	Top sand wave	0.227	0.273	0.347

The Zandvoort data is from Van de Meene and Van Rijn (2000).

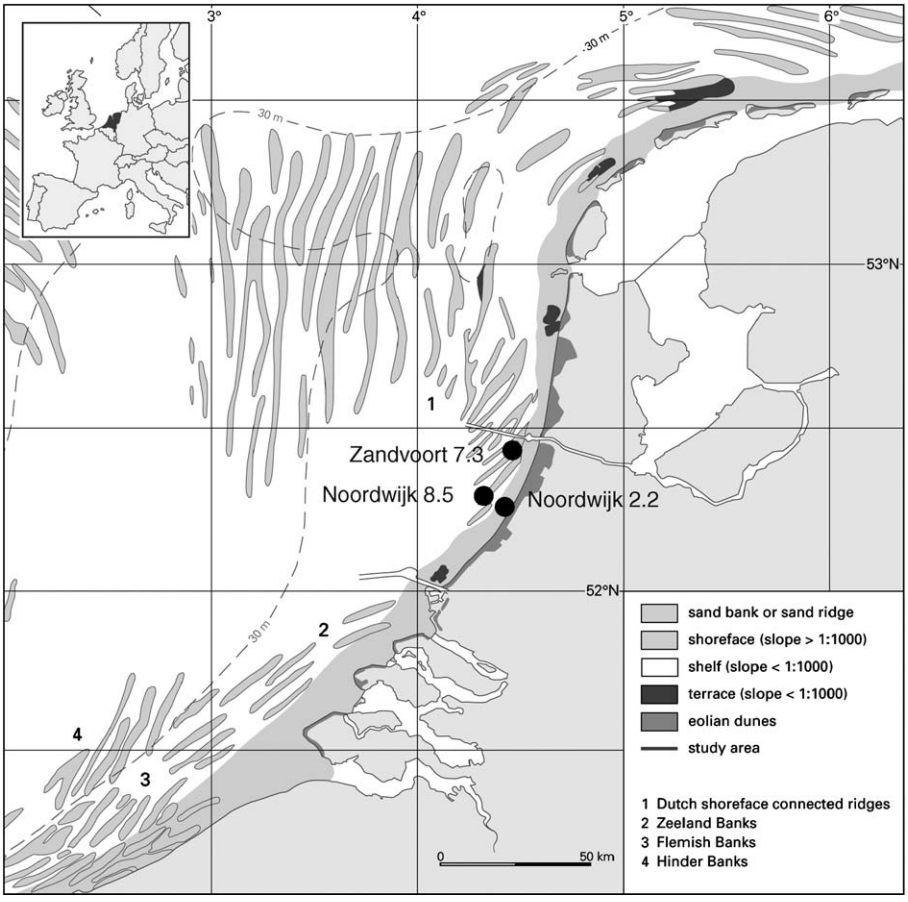

Fig. 1. Morphological map of the North Sea off The Netherlands with tidal and shoreface-connected ridges and the shoreface (after Van de Meene and Van Rijn (2000)) The measurement positions are given as ●. Inset map shows the position of The Netherlands in Europe. (Courtesy Margot Stoete, Kartlab, Utrecht University).

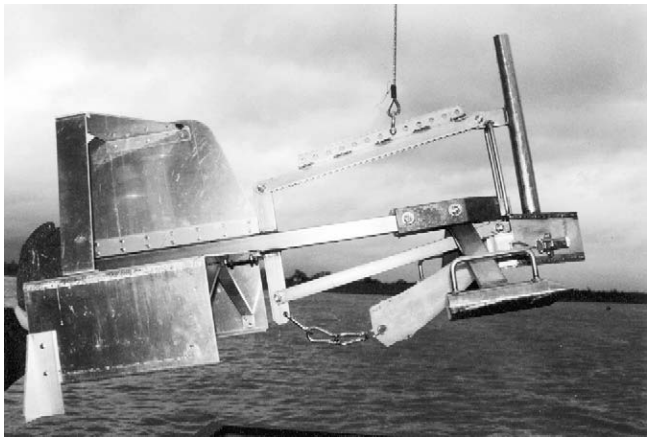

Fig. 2. The Nile sampler. The nozzle (≈ 10 cm wide) with the mesh bag is to the right (the vertical pole is for mounting velocity sensors), the box vane (with gloved hand for scale) to the left. Note the construction of the free-movable nozzle, which lands on the bed only after the box vane legs have dug into the bed and the front legs have landed (Van Rijn and Gaweesh, 1992). (Photo courtesy Roy Frings.)

The bed load transport rate was measured with a basket-type bed load 'Delft Nile' sampler (Fig. 2) (Van Rijn and Gaweesh, 1992) during two spring tidal flood peaks and one ebb peak in each campaign. This sampler has a nozzle of 0.095 m wide and 0.05 m high with a nylon sampling bag with mesh 0.15 mm with a patch of 0.5 mm on top to allow water and mud to escape and prevent blocking. The nozzle of the sampler is completely free of connections to the frame except at the nozzle top where it does not affect the near-bed flow. In addition, the nozzle is the most upstream part of the sampler, so that legs and other constructions do not affect the near-bed flow. The nozzle has a slightly downstream upsloping floor so that the nozzle entrance rests on the sand but the floor of the nozzle barely does, so a small shell or stone under the nozzle will not lift it above the sediment. The nozzle is also sharpened at the front so that it does not cause much turbulence which could lead to scour. Most importantly, the nozzle is connected to the frame in a movable way. When the sampler is suspended from the winch cable, the nozzle is lifted above the bottom level of the box vane and the forelegs. So, when the sampler lands on the bed, it first lands the box vane (assuming that the suspended sampler is slightly out of equilibrium with the box vane at a lower level than the forelegs), then the forelegs, and finally, when the cable is further released, it lands the nozzle. In this way any sediment that is suspended in the landing is not sampled, and any initial movements made by the sampler over the bed before the hind legs dig into the bed do not cause dredging by scraping over the bed.

The bed load transport rate is determined from the measurements as:

$$q_b = \alpha \frac{(1-\lambda)(V-V_0)}{wt} \tag{1}$$

in which α=calibration coefficient, defined as true divided by sampled transport, λ=0.38 pore space of the sediment in the graded cylinder with which the sample volume V is determined, V_0=zero sampling volume (explained below), w=sampler nozzle width and t=sampling time. The laboratory calibration factor of the Nile sampler is 1.0±0.2 (error represents 95% interval) (Gaweesh and van Rijn, 1994) (Fig. 3). This indicates that the instrument works very well compared to other bed load samplers such as the Helley Smith, which have much larger calibration coefficients indicating under-sampling (Emmett, 1980; Hubbell, 1987; Thomas and Lewis, 1993). The finest sediment and smallest flow velocities in the calibration was similar to the present measurement conditions (Fig. 3).

In all cases where the sampler is deployed from a ship, it is very important that the ship is well-fixed onto its position. Any movement of the ship will cause extra drag on the cable, which may lift the nozzle from the bed, or, worse, drag the sampler over the bed. Such drift will cause dredging of bed material into the nozzle. At the shallow sites the ship was anchored and used only little power for dynamic positioning based on GPS. At the deeper site anchoring was not stable enough and the dynamic positioning was used, but care was taken to suspend the sampler

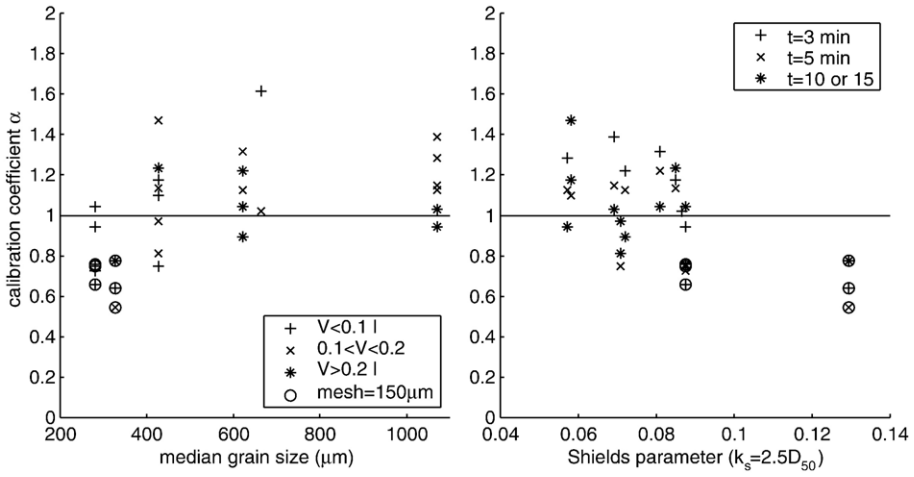

Fig. 3. Calibration of the DNS based on data in Gaweesh and van Rijn (1994). The calibration coefficient is plotted against median grain size (D_{50}) and the Shields parameter related to grain roughness (k_s=2.5 D_{50}, explained later), and the data are classified for sample volume V (in liters) and sampling time t (in min). All experiments were done with a mesh bag of 250 mm except those indicated with 'mesh=150 mm'. Each point represents 30–300 samples.

from a long crane as far from the side of the ship as possible. The sampler was carefully placed on the bed, and the effect of the landing was quantified independently by measuring the sampled volume after landing and lifting five times (to capture enough) with a sampling duration of <1 s. This duration need not be larger, as laboratory and video observations by Van Rijn and Gaweesh (1992) showed that the scooped and stirred sediment, if any, was captured immediately because it is caused at the entrance of the nozzle. The zero sampling volumes (divided by 5) in the measurements presented here were of the order of <1 ml whereas the bed load samples had volumes of about <30 ml (ignoring zero transports which are considered sampling errors caused by, e.g. the sampler nozzle to rest on a large shell). The zero sampling volume was subtracted from the bed load samples to account for sediment stirred and scooped up in the landing and lifting of the sampler (Gaweesh and van Rijn, 1994). The sampling durations of bed load transport were between 10 and 40 min depending on the current velocity.

The hydrodynamics were measured with two instrumented tripods deployed at 2 km offshore: the HSM-tripod ('Hydrodynamics, Sediment transport and Micromorphology'-tripod) and the Hydro-tripod (measuring hydrodynamics only). All instruments operated in burst mode with a frequency of 2 Hz and a burst duration of 34 min. The HSM-tripod measured flow velocity with 7 electromagnetic current sensors in spring and 3 in autumn, in both cases distributed between 0.05 and 1.1 m above the bed, and measured pressure. In addition, a ripple profiler gave an impression of the bed surface dynamics due to bed forms. The HSM-tripod was deployed for 4 weeks in spring and 6 weeks in autumn. In addition, almost 1 year [>8000 h] of data was collected with an electromagnetic current sensor an a pressure sensor at a height of 0.32 m above the bed on the Hydro-tripod, also at 2 km offshore, between March 2003 and March 2004. The distance between the Hydro- and HSM-tripods is about 70 m but comparison of the data demonstrated excellent comparability of current and orbital velocities within the accuracy of the sensors.

The flow velocity was also measured with one or two OTT propellor type current meters mounted on the bed load sampler. These measurements served as a check whether the flow velocity was the same as measured at the tripods. In the Van de Meene and Van Rijn (2000) data the velocities were measured with three OTT current propellors on the bed load sampler, and tripod data was unavailable.

The wave climate is represented by 30 years of wave measurements at a platform 9.5 km off the coastline. Comparison of the wave height and period probability distributions for the full 30 year dataset and for the burst numbers of Hydro-tripod data demonstrates that the Hydro-tripod data is representative for the climate (not shown), except the two largest storms of the past 30 years which did not occur in the tripod measurement period. These two storms do not have a significant effect on annual transport rate because the effect of wave stirring on net annual transport is limited (Section 4).

A ripple profiler on the HSM-tripod and box-cores collected data on the characteristics of bed forms. In storms, rounded bed forms with heights of only a few cm developed. During the bed load measurements the bed sampled with the box-corer was nearly plane (maximum ripple height <0.005 m with ripple lengths of ≈ 0.01 m) (see example box-cores in Passchier and Kleinhans, 2005). This means that no flow separation took place over these bed forms and that the bed load sampling was unaffected by bed forms. Bed forms will not further be discussed here, because the shear stress calculation (given later) is independent of bed forms.

2.2. Current shear stress

The time- and depth-averaged velocity u was determined by a fit to the EMF data assuming the law of the wall up to the water surface:

$$u_c = \frac{u*}{\kappa}\ln\left[\frac{z}{0.033\ k_{sc}}\right] \tag{2}$$

where u^*=shear velocity, κ=von Kármán constant (0.4), k_{sc}=Nikuradse current-related roughness and z=height above the bed. The depth-averaged flow velocity is found at a height of (1/e) $h \approx 0.368h$, where h=water depth and e=Euler constant. This method gives slightly larger depth-averaged current velocities than the method of Soulsby (1997) where the law of the wall is fitted to a lower portion (of arbitrary height, e.g. the estimated boundary layer thickness) of the velocity profile and a vertical line above the lower portion. However, no EMF-sensors were available above ≈ 1.1 m above the bed so this method was not used.

The current shear stress related to grains was calculated following the concept of Van Rijn (1984a) as:

$$\tau_c = \rho g\frac{u_c^2}{C^2} \tag{3}$$

where ρ=density of water and C=Chézy grain roughness. The C is given as:

$$C = 18\log\frac{12h}{k_{sc}} \tag{4}$$

where h=water depth. A grain roughness of $k_{sc}=D_{90}$ is assumed, with D_{90}=90% percentile of the (cumulative) grain size distribution by mass. In the method of Ribberink (1998), the current shear stress has to be calculated as

$$\tau_c = \frac{1}{2}\rho f_c u_{c\delta}^2 \tag{5}$$

where $u_{c\delta}$=current velocity at height δ=0.01 m above the bed as specified by Ribberink. Note that our lowest EMF in the HSM-tripod was <δ. The f_c follows from Eq. (2) as:

$$f_c = 2\frac{0.4}{\ln\frac{\delta}{0.033k_{sc}}} \tag{6}$$

where k_{sc} is assumed to be 0.1 m (discussed later). In all cases hydraulic rough conditions are assumed, which was defined as

$$\mathrm{Re}_* = \frac{u_* k_{sc}}{\nu} \geq 11.63 \tag{7}$$

in which ν=kinematic viscosity of water ($\nu \approx 1.2\cdot 10^{-6}$ m^2/s).

2.3. Wave shear stress and wave stirring

The grain-related shear stress for waves is calculated as

$$\tau_w = \frac{1}{2}\rho f_w U_{rms}^2 \tag{8}$$

where U_{rms}=rms orbital velocity amplitude, calculated as $U_{rms} = \sqrt{2}(U_{rmsX}^2 + U_{rmsY}^2)^{1/2}$ where U_{rmsX}^2 and U_{rmsY}^2 are determined as the burst average of the squared 2 Hz signal of velocity in cross-shore and alongshore direction, respectively. The f_w is calculated with the *Swart* equation:

$$f_w = \exp\left[-5.977 + 5.213\left(\frac{A_{rms}}{k_{sw}}\right)^{-0.194}\right] \tag{9}$$

A grain-related wave roughness of $k_{sw}=2.5D_{50}$ is prescribed for this equation. The A_{rms}=near-bed orbital amplitude calculated from $A_{rms}=(U_{rms}T_{rms})/2\pi$ where T_{rms}=is the period determined from the pressure signal.

Wave stirring is calculated with the method of Ribberink (1998), which is similar to the more recent method proposed by Soulsby and Damgaard (2005) and was tested on a similar dataset. The wave-current interaction is then incorporated in a combined-flow friction factor for the instantaneous (intra-wave) velocity vector:

$$f_{cw} = \gamma f_c + (1-\gamma) f_w \tag{10}$$

in which the wave friction is calculated with Eq. (9) and $\gamma = U_{c\delta}(U_{c\delta}+U_{rms})^{-1}$. The current friction parameter (Eq. (6)) is calculated for the near-bed velocity at height δ, which was determined from the measured velocity at a much larger height, an assumed apparent roughness of 0.1 m and the logarithmic velocity profile. An instantaneous velocity vector is calculated from the time-averaged alongshore current and a sine wave with amplitude U_{rms} constructed at 10 Hz with the T_{rms} from the pressure signal. The instantaneous transport is calculated from the instantaneous velocity vector and the time-averaged friction factor for waves plus currents, then decomposed into cross-shore and alongshore transport and then averaged over the wave for the alongshore direction (Ribberink, 1998).

2.4. Sediment transport predictors

The dimensionless shear stress ('Shields parameter') is calculated as:

$$\theta = \frac{\tau}{(\rho_s-\rho)gD_{50}} \tag{11}$$

The sediment transport is expressed in non-dimensional form ('Einstein parameter') as

$$\phi = \frac{q_s}{(Rg)^{1/2}D_{50}^{3/2}} \tag{12}$$

wherein $R=(\rho_s-\rho)/\rho$ is relative submerged density of sediment, q_s=sediment transport rate ($m^3m^{-1}s^{-1}=m^2/s$). Common bed load sediment transport predictors are all of the following forms (Meyer-Peter and Mueller, 1948; Fernandez Luque and Van Beek, 1976; Parker et al., 1982; Van Rijn, 1984a; Wilson, 1987; Nielsen, 1992; Ribberink, 1998; Soulsby and Damgaard, 2005):

$$\phi = \alpha(\theta-\theta_{cr})^{\beta_1} \tag{13}$$

$$\phi = \alpha\left(\frac{\theta-\theta_{cr}}{\theta_{cr}}\right)^{\beta_1} \tag{14}$$

$$\phi = \alpha\frac{(\theta-\theta_{cr})^{\beta_1}}{\theta_{cr}^{\beta_2}} \tag{15}$$

$$\phi = \alpha\theta^{\beta_1} \tag{16}$$

$$\phi = \alpha\sqrt{\theta}(\theta-\theta_{cr}) \tag{17}$$

where α=empirical constant of $O(1–10)$ and $\beta_1 \approx 1.5$, or 4.5 with $\beta_2=3$ for Eq. (15) (Table 2). In Van Rijn (1984a) the transport rate also depends on dimensionless grain size as $D*^{-0.3}$, which is independent of shear stress and therefore constant for a given sediment size. This *Bonnefille* dimensionless grain size is defined as (in Van Rijn, 1984a):

$$D_* = D_{50}\sqrt[3]{\frac{Rg}{\nu^2}} \tag{18}$$

The critical shear stress of sediment may be affected by various factors, for example the effect of the chosen grain roughness length in the Shields parameter calculation, the calibration of the bed load sampler or the effect of cohesion due to mud in the sediment, cementation or compaction by benthic

Table 2
Coefficients in bed load predictors

Predictor	Form	α	β_1	β_2	θ_{cr}
Meyer-Peter and Mueller (1948)	13	8	1.5		0.047
Fernandez Luque and Van Beek (1976)	13	5.7	1.5		0.03
Parker et al. (1982)	15	11.2	4.5	3	0.5 $\theta_{cr,Shields}$
Van Rijn (1984a)	14	0.1	1.5		$\theta_{cr,Shields}$
Wilson (1987)	16	12	1.5		$\theta_{cr,Shields}$
Nielsen (1992)	17	12			0.05
Wiberg and Smith (1989)	13	1.6 ln (θ)+ 9.8	1.5		$\theta_{cr,Shields}$
Ribberink (1998)	13	11	1.65		$\theta_{cr,Shields}$
Soulsby and Damgaard (2005)	17	12			$\theta_{cr,Shields}$
This paper ('North Sea predictor')	13	1	1.5		0.5 $\theta_{cr,Shields}$

The form of the predictor is given by reference to equation numbers.

animals. This will be discussed in Section 4. The Shields curve model of Zanke (2003) is used to calculate the theoretical critical Shields value as $\theta_{cr}=\alpha_{cr}\theta_{Zanke}$. The parameter $\alpha_{cr}=1$ in the original model, representing a certain probability of transport where grain collisions occur frequently, but is here taken as 0.5 for low transport rates around the beginning of individual particle motion following Parker et al. (1982).

Since the bed load transport at the field site is very near the beginning of motion, the fit of an empirical predictor to the data is affected by the criterion for initial motion. Fluctuations in the flow due to turbulence provide a mechanism for transport in conditions below the criterion. To account for this, a simple stochastic approach to turbulence can be applied to any of the above mentioned predictors or an empirical predictor (Kleinhans and Van Rijn, 2002). This also allows fitting an empirical predictor to measurements just above and below the criterion. The transport is calculated for a range of τ_{ci} below and above the average τ_c. The calculated transports ϕ_i are multiplied with the probabilities p_i of occurrence of all the τ_{ci} in the distribution of shear stress. In this paper we use a Gaussian distribution parameterized by the average τ_c and the standard deviation $\sigma_\tau=0.4\tau_c$ (Kleinhans and Van Rijn, 2002):

$$p_i = \Delta\frac{\tau_c}{\sqrt{2\pi\sigma_\tau}}\exp\left[-\frac{1}{2}\left(\frac{\tau_{ci}-\tau_{cr}}{\sigma_\tau}\right)^2\right] \tag{19}$$

for the discrete normal distribution with class width Δ. The distribution is discretized for $-6\sigma_\tau \le \tau_c < 6\sigma_\tau$ which amply covers all significantly contributing fluctuations. The sum of the products represents the cumulative bed load transport due to turbulent fluctuations:

$$\phi = \sum p_i\phi_i \tag{20}$$

for non-zero transports ϕ_i in both up-drift and down-drift direction, which implies calculation only for $|\tau_{ci}|>|\tau_{cr}|$.

The empirical probability distribution of velocity fitted well to a normal distribution. The instantaneous τ_{ci} were logarithmically distributed with $\sigma_\tau=0.28\tau_c$. For fluvial conditions this factor is known to be about 0.4 (Kleinhans and Van Rijn, 2002) from measurements with a high enough frequency to cover the full turbulence spectrum, whereas in this paper the sampling frequency was low (2 Hz), so 0.4 is assumed below. However, see the discussion (Section 4) on turbulence damping by mud.

2.5. Integration to annual bed load transport

Upscaling of the bed load measurements to the annual wave and current climate is done as follows. The depth-averaged current velocity is determined from fitting all HSM sensors between 0.05 and 1.1 m to the law of the wall for 10 weeks of data. These depth-averaged velocities are correlated to the velocities measured simultaneously at a single height in the Hydro-tripod, which relate as $u_{HSM}=1.4u_{Hydro}$. The scatter in the relation is caused by time-varying hydraulic roughness due to bed forms, wave-current interaction and sediment transport. The apparent roughness length derived from the law of the wall and HSM sensors varied between 0.02 and 0.35 m. It is difficult, however, to determine a trend of roughness with the conditions and with the dimensions of bed forms. This lead Houwman and Van Rijn (2002) to the conclusion that using a roughness length of 0.1 m is as good an approach as to use roughness and bed form predictors. This uncertainty is expressed here as a variation of the multiplication factor between u_{HSM} and u_{Hydro} of 1.1–1.7 To assess the effect of the scatter, these multiplication factors are applied to the sediment transport calculations later. The scatter does not affect the derivation of the empirical bed load predictor because for this the HSM-tripod data or the propellor-type current meters were used. If, however, there were a systematic relation between the roughness length and the angle between the currents and waves as found in laboratory experiments (Kemp and Simons, 1983; Fredsoe et al., 1999), then the present method will be biased slightly. This topic must therefore be further investigated in field measurements.

The resulting approximation of depth-averaged velocity is then applied to the full year of Hydro-tripod data. A probability distribution of these velocities was calculated. This probability distribution was then applied to the bed load predictors by computing sediment transport for each velocity class and multiplying that transport rate with the probability of that velocity class. After summing over all classes the result is an estimate of alongshore annual bed load transport:

$$q_{annual} = \sum_i \sum_j p_{u_c,i} p_{U_{rms},j} q_{i,j} \tag{21}$$

for current velocity pdf classes i and orbital velocity pdf classes j. For the wave stirring method the Hydro-tripod data is used to calculate an empirical probability distribution of orbital velocity of the rms wave heights and peak orbital motions for a full year.

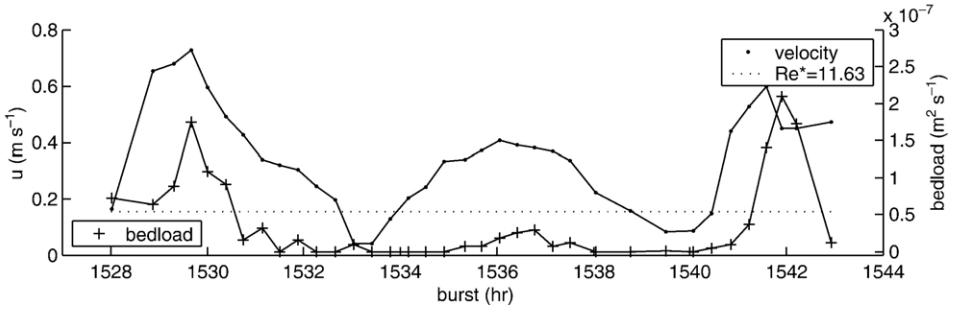

Fig. 4. First time series of bed load at Noordwijk 2.2 km offshore, spring data, waves smaller than 0.5 m. Large velocity peaks are flood currents, smaller (middle) is the ebb current.

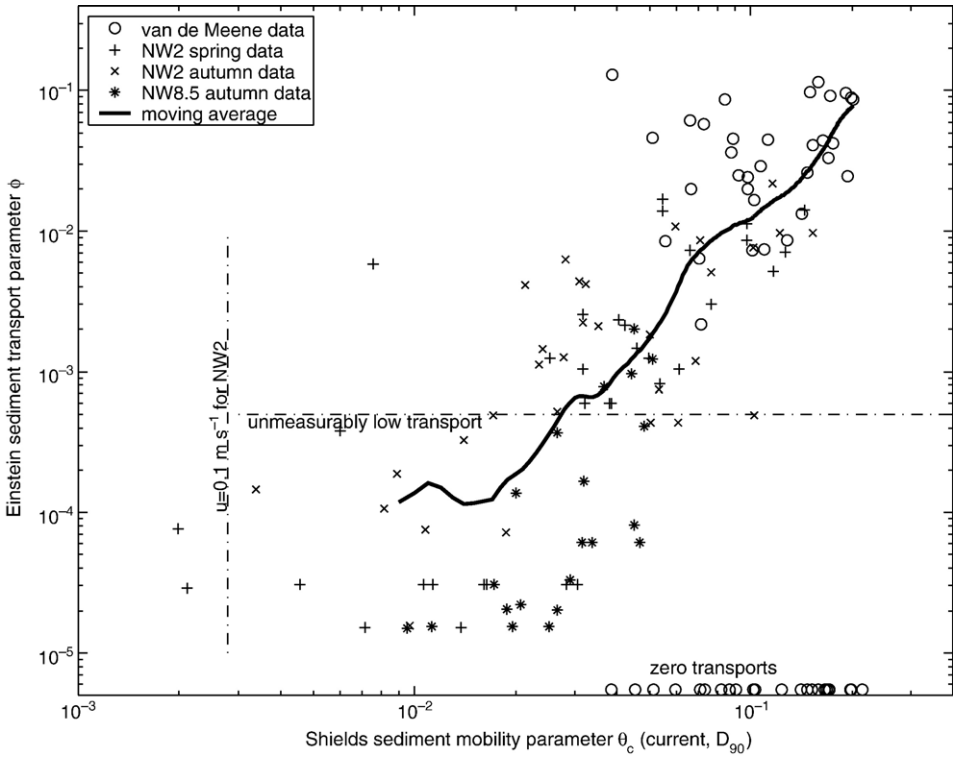

Fig. 5. Dimensionless bed load *versus* shear stress of the data and moving average. Limits of observability are given.

The probabilities for ebb currents (southward) are larger than for flood currents, but this is more than counterbalanced by the larger peak velocities of flood currents, resulting in a small net northern drift. Tidal water depth variations were ignored which can safely be done as the variations are at most 10% while water depth only affects the results through the roughness predictor.

The annual transports were calculated for an empirical predictor and for the Van Rijn (1984a) predictor for currents only and

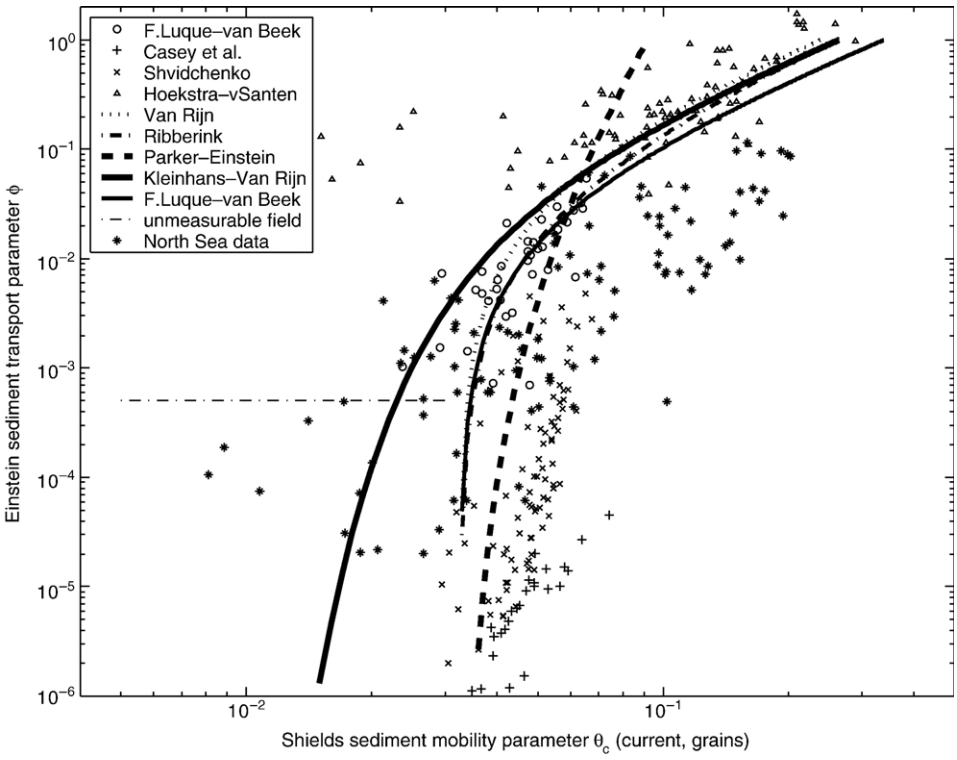

Fig. 6. Comparison of dimensionless transport data to other data and transport predictors (see Table 3). The dimensionless shear stress for the *Hoekstra-vSanten* data (see text) is calculated with the wave-current interaction method of Soulsby (1997).

Table 3
Experimental data-sets of bed load near incipient motion of uniform sediment, and one field data set

Reference	D_{50} (mm)	$\theta_{ref,empirical}$	$\theta_{cr,Zanke}$	Remarks
Fernandez Luque and Van Beek (1976)	0.9, 1.8, 3.3	0.019	0.035–0.055	35 experiments, natural sediments
Shvidchenko et al. (2001)	1.5–9	0.060	0.056–0.080	86 experiments, only $h/D_{50}>10$
Casey et al. (1935, in Shvidchenko et al. (2001))	2.46	0.083	0.073	35 experiments, only $h/D_{50}>10$
Hoekstra et al. (2004)	0.29 ($D_{90}=0.60$)			89 field cases

The modelled critical Shields parameter was calculated for individual experiments and given as a range.

for the full climate including wave stirring. This was also done for the velocity probability distribution used by Van Rijn (1997) to demonstrate the effect of a misrepresentation of the current climate. The effect of using different upscaling factors between the HSM- and Hydro-tripod velocities is also demonstrated.

3. Results

3.1. Measured bed load

The velocities measured with different instruments give comparable results. In addition, there is a strong correlation (not shown) between the depth-averaged velocity calculated from the logarithmic profile fit and the velocity at one single height of 0.32 m (factor 1.4 smaller than depth-averaged), indicating that the hydraulic roughness does not have much effect on the depth-averaged current. Box-core samples and ripple profiler measurements (not reported here) revealed that the bed was nearly plane with very shallow, smoothed relic bed forms during all measurements (see examples in Passchier and Kleinhans, 2005).

A typical time series of burst-averaged tidal current velocity and bed load transport (Fig. 4) shows that significant sediment transport mostly occurs in the largest flood velocities. The bed load transport rates as a function of shear stress, both in dimensionless form, show a trend with a factor of 5 scatter (Fig. 5). Below a dimensionless transport rate of 5×10^{-4} the scatter increases, because this is a sampled bed load volume of about 1 ml in 20 min which is equal to the zero sampling volume. Therefore this transport rate will be called the limit of measurable transport.

The quality of the samples of Gaweesh and van Rijn (1994) was controlled by video observations or by a rule of thumb to remove outliers. This was impossible in the present field measurements because the seawater was opaque to the video and mounting the video too near to the nozzle would have disturbed the flow. Therefore we present all the data including the points we suspect to be outliers. Despite the scatter, the trend below and above the limit of measurable transport is similar, as indicated by the moving average. The moving average was calculated on the logarithmical transforms of the dimensionless transport and

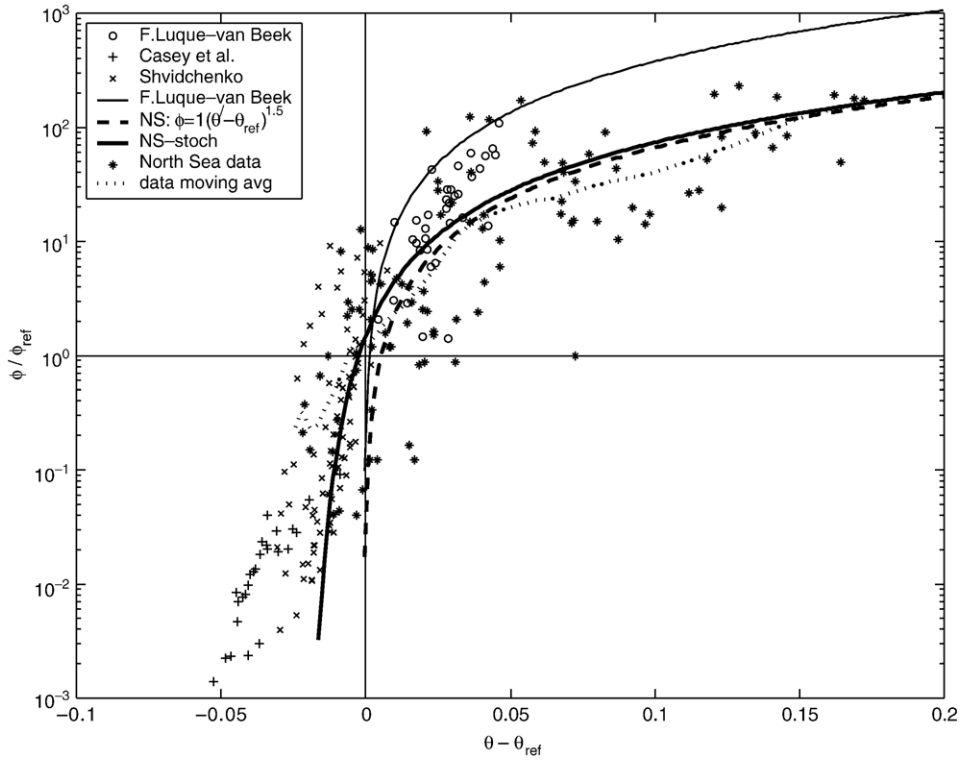

Fig. 7. Similarity collapse of the data. Dimensionless transport and Shields parameter are plotted relative to the critical/lowest measurable values. The stochastic version of the North Sea predictor predicts sediment transport below the critical Shields parameter. Note the difference between the Fernandez Luque and Van Beek data and the Fernandez Luque and Van Beek predictor, which is due to the different method and criterion for the calculation of the critical Shields parameter.

shear stress because transport predictors are power functions of the dimensionless shear stress. The transport samples below the limit of measurable transport are not considered reliable. In addition, the zero transport values have been removed in the calculation of the trend line, because, given the long sampling time, it is likely that these represent sampling problems rather than true zero transports (see Section 2.1). For example, if the sampler nozzle rests on a large shell, the sediment will pass under the nozzle. Most of the zero transport values occur in the data of Van de Meene and Van Rijn (2000).

As a check, the suspended load concentrations were measured by suction on 25 September 2003 (Table 1). These remained below 0–6 mg/l (one exception of 20 mg/l which may be an outlier) just above the bed load sampler nozzle for a current velocity of 0.7 m/s. This demonstrates that suspended sediment load captured in the bed load sampler was negligible during the measurements in agreement with Van de Meene and Van Rijn (2000), so the sampled sediment is bed load transport only despite the nozzle height of 0.05 m of the sampler. (These measurements are not further reported here.)

3.2. Transport near the beginning of motion

The limit of measurable sediment transport in the field is shown in Fig. 5. The intersection of the trend through the data and this line of so-called reference transport ϕ_{ref} is a measure for the critical Shields mobility, which here is $\theta_{ref} \approx 0.03$ in excellent agreement with the Zanke model with $\alpha_{cr}=0.5$, which predicts $\theta_{cr}=0.03$. The collapse of the data on a single transport function therefore depends on the critical shear stress as well as the actual (grain) shear stress.

The effect of chosen roughness length on empirical reference Shields values (θ_{ref}) is limited to 20%, with $3D_{90}$ giving the largest dimensionless shear stress, $1D_{90}$ the smallest and $2.5D_{50}$ in between. (All data points shift along the x-axis with the same factor in Figs. 5 and 6). The reason for this small effect is that the sediment has a narrow grain size distribution so the D_{90} is not much larger than the D_{50}.

It is useful to compare the present data to other data sets of bed load transport very near incipient motion conditions (Table 3 and Fig. 6), even though these differ in other respects such as grain size. The bed was nearly plane in all conditions and the grain roughness is (assumed to be) D_{90}. The Zanke (2003) model accounts for a water depth effect: the critical Shields parameter significantly increases with $h/D_{50}<10$ due to decreasing turbulence, wherein h=water depth, which accounts well for the rather large critical Shields parameters of the laboratory data (Table 3).

Hoekstra et al. (2004) presented bed load transport data in waves plus currents far above incipient motion in both wave and current dominated conditions over an ebb-tidal delta. The

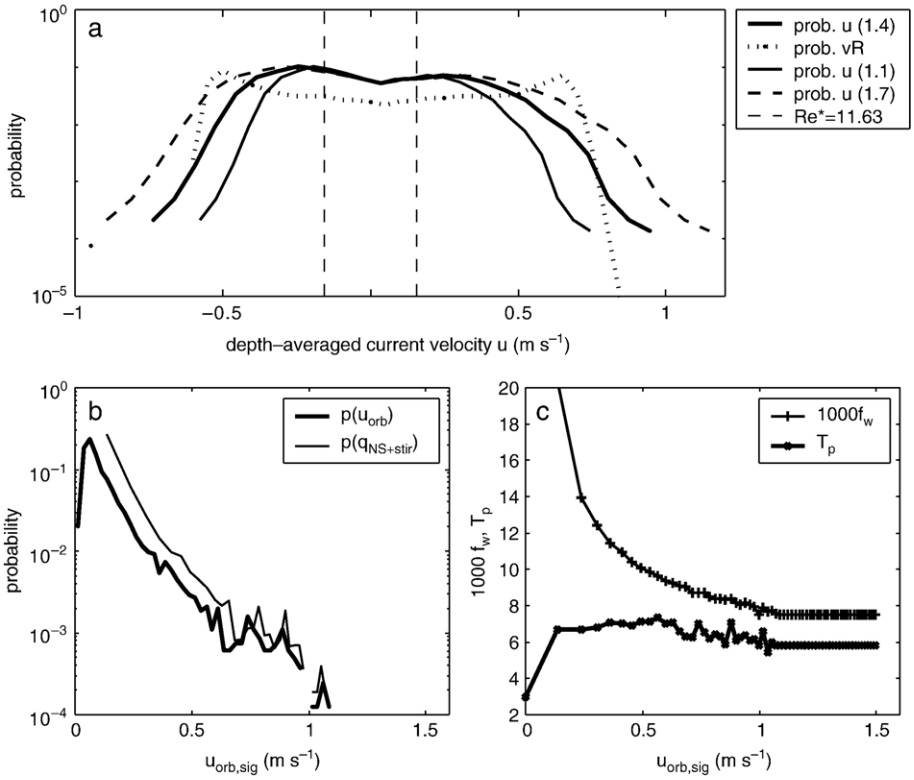

Fig. 8. Current and wave climate at Noordwijk 2.2 km. a. The probability distributions of depth-averaged current velocity according to the HSM-and Hydro-tripods and the probability distribution of Van Rijn (1997). The numbers 1.1, 1.4 and 1.7 indicate the factor between the depth-averaged HSM velocity and the local Hydro point velocity. Positive current and transport are in the flood direction. The transition between hydraulic smooth and rough conditions is indicated. b. Orbital significant peak flow climate at Noordwijk 2.2 from the Hydro-tripod, and the probability of sediment transport calculated with NS and wave stirring (summed over all current velocities). c. Average f_w friction factor (multiplied with 1000) and T_p period of the orbital velocity classes in b.

dimensionless shear stress including wave-current interaction is calculated with the two-parameter model of Soulsby (1997). Although with considerable scatter, the data follow the trend and magnitude of most bed load predictors.

3.3. Measured and predicted bed load transport rate

To account for the differences in critical shear stress of the data sets the dimensionless data are further normalized by dividing the actual shear stress with critical shear stress and the actual transport rate with the minimum observable transport rate (chosen equal for all data). This removes the effect of the critical shear stress and the chosen reference transport rate from the graph, so that only the shape of the transport predictors is compared. The data now collapse rather well (Fig. 7) and the transport functions can now be tested and an empirical function will now be fitted.

The North Sea data are generally over-predicted with a factor of 5 by most predictors (Fig. 6). Considering the scatter it is not useful to discuss the intricacies of these bed load predictors. The Parker et al. predictor was found to predict well for gravel-bed rivers near incipient motion, but misrepresents the trend of the North Sea measurements. The empirical fit to the North Sea data (hereafter called North Sea predictor) is reported in Table 2. The effect of differences in reference shear stress was removed by plotting the excess dimensionless shear stress. After doing this, the North Sea predictor predicts the data rather well within a factor of 5 (Fig. 7). The scatter in the data does not merit further refining of the predictor.

3.4. Annual transport rate

The annual transport rates were calculated by integrating the transport rates calculated for each velocity bin in the velocity probability distributions (Section 2.5). Figs. 8 and 9 show the probability distributions of flow and of sediment transport for various combinations. These distributions are integrated for the ebb and flood direction; the difference is the net transport (Table 4).

The Van Rijn and Ribberink predictors yields 5–10 times larger transports than the North Sea predictor in all cases as can be expected from the difference between the predictors. The stochastic predictor was necessary for a better fit to the data but in the presence of wave stirring it is irrelevant.

The effect of wave stirring is an increase of 2–3 times of the flood and ebb transports. The cause is that wave stirring enhances the shear stress enough to overcome the critical shear stress for motion, even when the time-averaged current shear stress is below the incipient motion criterion. For infilling of sand extraction pits the flood and ebb transports are probably more important than the net transport, so wave stirring is very relevant.

The effect of the uncertainty in the upscaling of Hydro-tripod point velocities to depth-averaged HSM-tripod flow velocities due to natural apparent current roughness variations is studied by applying different multiplication factors of 1.1 and 1.7. These factors cause the annual transport to vary with a factor of 1.6–2 (Table 4), which is small compared to the uncertainty in the sediment transport predictors.

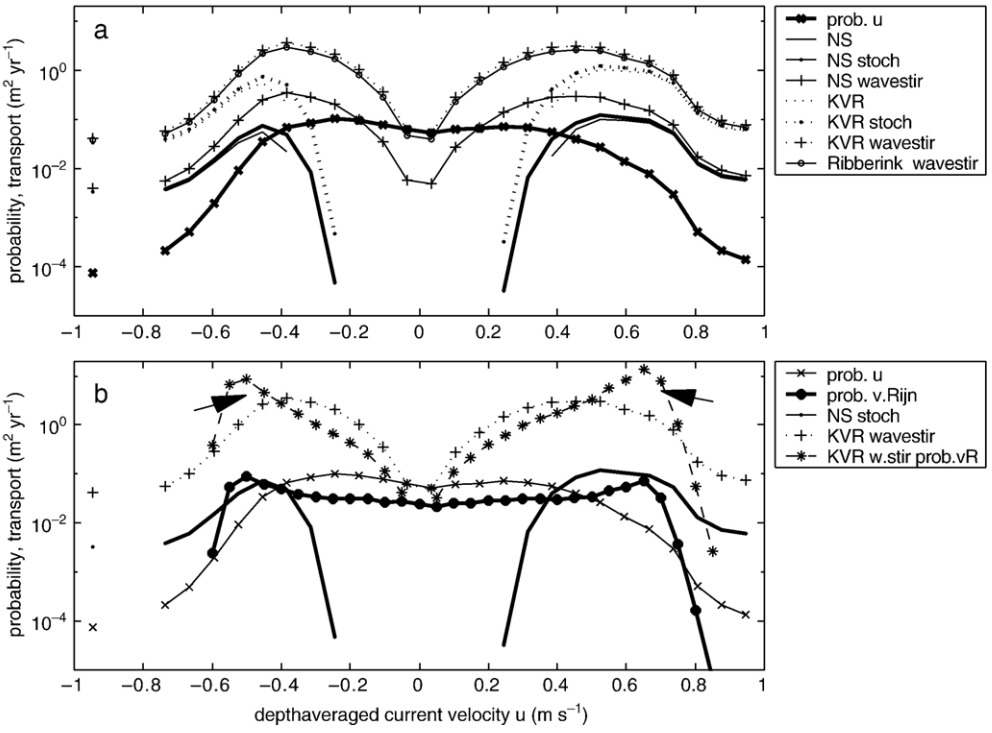

Fig. 9. a. Sediment transport predictions with the North Sea bed load predictor, the Kleinhans and Van Rijn (2002) (KVR) and the Ribberink (1998) for the measured climate (transport in m^2/year/velocity bin). The (KVR) generally overpredicts a factor of 10 compared to the North Sea (NS) predictor. b. Summary of a., with predictions with KVR with the probability distribution of Van Rijn (1997). Arrows indicate the part of the distribution that causes the much larger gross and net annual transport rates.

Table 4
Comparison of calculated annual bed load transports m^2/year at Noordwijk 2.2 km offshore for the Van Rijn and North Sea predictors

Predictor	Module	Measured flow		Net	Van Rijn et al. (2005b)		Flow
		Flood	Ebb		Flood	Ebb	Net
Van Rijn (1984a)	Basic	4.41	−1.38	3.03			
	Wave stirring 1.4	18.50	−14.09	4.41			
	Wave stirring 1.4 $U_{1/3}$	30.35	−24.97	5.38	47.70	−27.31	20.39
	Wave stirring 1.1	10.73	−8.52	2.21			
	Wave stirring 1.7	29.72	−21.83	7.89			
Ribberink (1998)	Wave stirring 1.4	15.51	−11.65	3.86			
	Wave stirring 1.4 $U_{1/3}$	27.43	−22.31	5.12	40.70	−22.91	17.79
	Full signal	20.23	−17.14	3.10			
This paper	Basic	0.43	−0.13	0.30			
	Wave stirring 1.4	1.77	−1.35	0.42			
	Wave stirring 1.4 $U_{1/3}$	2.91	−2.39	0.52	4.57	−2.62	1.96
	Wave stirring 1.1	1.03	−0.82	0.21			
	Wave stirring 1.7	2.85	−2.09	0.76			

For the factors 1.1, 1.4 and 1.7 for wave stirring see Fig. 8.

The year of Hydro-tripod data represents the wave climate data well except for the very largest storms of the past 30 years (not shown). However, the relative contribution (probability) of those transports to the annual transport rate is $p(q_{NS}+\text{stir})<0.001$ (Fig. 8, because both large waves and small waves are able to stir the sediment, whereas the current is the limiting factor in the averaged flood, ebb or net transport rate. The largest storms may, however, still have a large effect on the suspended load transport but that is not the scope of this paper.

In general, the transport by flood currents is 1.5–3 times larger than by ebb currents, with the largest differences for the basic predictors and the smallest for the wave stirring options. The calculated net annual transport rates with all methods range between 0.2 and 20 m^2/yr. The large differences are mostly due to the differences between the existing and empirical bed load predictors. The net transports are the subtle differences between much larger flood and ebb-related transport rates. If the North Sea bed load predictor is representative for the field sites then the net annual transport rate is 0.2–0.7 m^2/year; if the Van Rijn (1984a) or Ribberink (1998) predictor is representative then the net transport is 2.2–7.9 m^2/year.

4. Discussion

4.1. Test of bed load predictors

The deviation between existing transport predictors and the present measurements could be caused by an increase of the critical shear stress for incipient motion due to, for example, mud and sediment-binding biota. The Noordwijk sites have at most 5% mud in the bed (Kleinhans et al., 2005a). The effect of mud on incipient motion depends on the amount of clay in the sediment, on the type of clay, on the compaction of the sediment and floc size of the clay and on the sand grain size (Mitchener and Torfs, 1996; Panagiotopoulos et al., 1997). For a mud fraction of 10% the increase in critical shear stress is between a factor of 1–8, while the mud content at Noordwijk is only about 3%. However, the empirically derived critical shear stress is rather small and is the same as predicted by the Shields curve without cohesive effects. Yet, the interaction of mud and sand is poorly understood. The mud may also affect the flow by damping the turbulence, which Baas and Best (2002) found for kaolinite above a few percent of volume. At the field site, more complex clay minerals enriched with organic matter prevail of which the damping and cohesion effect is probably much stronger than for pure kaolinite clay. High mud concentrations of 0.1–1 kg/m were measured at the field site (Kleinhans et al., 2005a) which might have damped the turbulence and therefore decreased the bed load transport rate. Concerning biotic effects, benthic fauna such as bivalves and bristle worms is absent in spring and abundant in autumn (Kleinhans et al., 2005a). With the large uncertainty of the measured bed load transports it was not possible to identify a significant difference between the bed load samplings done in spring and in autumn.

Using a stochastic model representing the effect of turbulence was useful to derive an empirical bed load predictor. Not using the stochastic model would have resulted in a less well supported fit given the scatter and limited mobility range of the data. Moreover, the stochastic model represents the natural process better. The continuation of the trend of transport below threshold θ_{cr} shows that there is no real threshold but a gradual incipience region as is well known. For the Noordwijk site the time-averaged tidal θ_c is below critical for two-thirds of the time. Above θ_{cr} the stochastic predictor asymptotically approaches the non-stochastic predictor to which the stochastic module was applied. If a shear stress standard deviation of 0.28 rather than 0.4 were used then the transport predictor would be somewhat steeper below the critical Shields value, but the calculated transport rates are not very sensitive to this choice. The measured standard deviation of 0.28 is smaller than the 0.4 used in rivers, which may be indicative of turbulence damping. Although spectral analysis of the current signal demonstrates that most of the energy of the flow is contained in frequencies >0.5 Hz (Kleinhans et al., 2005b), the relatively large EMF sensors are unable to measure higher frequencies, which may have reduced the standard deviation. We speculate that the cause is turbulence damping by mud as found by Baas and Best (2002), but more dedicated field measurements are necessary to investigate this phenomenon.

The calibrated bed load equation fits reasonably well on other data sets for transport near incipient motion. This means that after accounting for differences in the critical Shields parameter, the North Sea stochastic predictor describes the data well enough considering the uncertainties in the data.

It is interesting to note that Wiberg and Smith (1989) provide a variable α depending on θ, which covers the validity ranges of Fernandez Luque and Van Beek (1976), Meyer-Peter and

Mueller (1948) and Wilson (1987) for increasing shear stress, respectively. The effect of this variable α could also be expressed as an increased coefficient β_1 while keeping α constant. By least-squares fitting, $\alpha=9.7$ and $\beta_1=1.67$ are obtained for $0.045<\theta<4$ with only 1.5% deviation between the fit and the original Wiberg and Smith function, which is remarkably close to Ribberink (1998). However, the Wiberg and Smith correction cannot explain the deviation between existing predictors and the present data.

The error in the calibration of the Nile sampler is not enough to account for the difference between the constant $\alpha=1$ with that of existing predictors. Suppose the calibration factor is underestimated by a factor of 2, which is in conflict with the much better results in Gaweesh and van Rijn (1994) and unpublished data at Utrecht, then this still does not explain the factor of 5 deviation of sediment transport. Moreover, other data sets near incipient motion collapse well on the North Sea function.

The comparison between the present data, the data from literature and the predictors demonstrates that (1) a universally valid predictor based on dimensionless shear stress only is not feasible, (2) much of the data are on average below values of most predictors, (3) that the present data set is not exceptional compared to other data sets, but (4) that the small transport rates might be caused by poorly understood interactions between mud and water and sand.

4.2. Annual transport rate

4.2.1. Effect of the current characteristics

The asymmetry between flood and ebb currents (reflected in the shape of the pdf) has the largest effect on the net annual transport. This is demonstrated by the Van Rijn (1997) estimate of annual net bed load transport rate at a water depth of 20 m at about 17 m^2/year. This is about five times as large as the value estimated in this paper (5.38 m^2/year, Table 4) with the same predictor of Van Rijn (1984a) and the velocity probability distribution derived from measurements. The cause is that Van Rijn (1997) and Van Rijn et al. (2005b) used a different probability distribution (Fig. 8), of which the source is not given but probably based on a model. The shape of this probability distribution differs from the measured one, especially for the larger velocities (Fig. 9). As a check, the misrepresenting distribution and the bed load predictor of Van Rijn (1984a) indeed yielded almost the same annual transport rate (20.39 m^2/year, Table 4) as Van Rijn (1997) ($\approx$ 17 m^2/year). This is a much larger effect than of any model component despite the uncertainties of sediment transport models. This dramatic difference emphasizes the need for an accurate current schematization based on field measurements in budget and model studies.

The calculation for the probability distribution of depth-averaged velocities in Van Rijn (1997) and Van Rijn et al. (2005b) is redone here for a few scenarios (last three columns of Table 4) to exclude the possibility that the difference in annual transport is caused by another difference in the calculation method. The misrepresentation of current climate leads to an over-prediction of the net transport of a factor of 5. Especially the flood-related transport is over-predicted. Both the asymmetry in flood and ebb transport and the over-prediction are caused by the areas of the probability distribution denoted by arrows in Fig. 9. Even in the unlikely case that the multiplication factor in the measured velocity upscaling were 1.7, the Van Rijn distribution still results in more than two times larger annual transport rates (7.89 m^2/year (upscaling factor 1.7) *versus* 20.39 m^2/year for Van Rijn, Table 4).

The uncertainty in the upscaling factor between depth-averaged current velocities derived from velocity profile measurements and local point velocities measured for a full year is probably due to variations in hydraulic ('Nikuradse') roughness lengths between 0.02 and 0.35 m (Kleinhans et al., 2005b). The effect on annual transport is less than a factor of two, which is much smaller than the uncertainty of the bed load predictor.

4.2.2. Effect of wave stirring

The effect of wave stirring increases the flood and ebb transports with a factor of 3–5 with the largest effect on the ebb-related transport. This is because the waves entrain the sediment when the current velocity is below the critical value for motion (central part of Fig. 9). The net transport, however, is of the same order as for the current without waves. Morphological change in reversing currents plus waves depends not only on the net transport but also on the gross transport rates, so it is useful to consider both net and gross annual transport rates.

For the calculations the rms orbital velocity was used, but it could be argued that the 1/3 highest waves (or the H_{m0} which is almost equal to the $H_{1/3}$ in the present data) represent the near-bed flow better for sediment transport purposes (e.g. Van Rijn et al., 2005a). For comparison, the annual sediment transport rate was also calculated from the mean of 1/3 largest near-bed oscillations for each burst, summarized in probability distributions in the same way as the rms velocities. The effect is an increase of almost a factor of two of the gross transports (18.50, −14.09 m^2/year for flood and ebb respectively, using the rms, *versus* 30.35, −24.97 m^2/year using the 1/3, see Table 4), while the net transport rate increases only slightly. In short, the waves determine the gross transport rate, but the asymmetry of the tidal current determines the net transport rate.

The annual transport calculation based on the probability distributions was compared to a transport calculation based on the measured instantaneous near-bed velocities. These were measured for almost a year so they also represent the combined wave and current climate well. The calculation was done with the Ribberink (1998) predictor exactly as specified in his paper. The full signal method predicts annual transport rates in between those calculated with the rms and 1/3 waves in the probability method (see values of the Ribberink method in Table 4). This indicates that an appropriate representative value of wave near-bed oscillations for transport calculations has an intermediate magnitude between the U_{rms} and $U_{1/3}$ for this area.

4.2.3. Effect of orbital flow asymmetry

In the full signal method the asymmetry between annual transport north and south is smaller than for the probability

distribution method. This leads to a smaller net transport rate of the full signal method (3.10 m^2/year, Table 4) than for the probability distribution method (3.86 m^2/year using the rms). One potential explanation is discussed below: wave orbital velocity asymmetry.

The wave orbital velocity asymmetry was small. (Orbital skewness and asymmetry have strict definitions differing from the simple method discussed below, but for the present purpose a loose definition is sufficient to observe a negligible effect of shoaling in the orbital velocities.) The near-bed orbital velocity in the alongshore direction was analyzed in the time-domain: the 1/3 largest waves were identified in both the flood (northern) and ebb (southern), (coast-parallel) directions and averaged to obtain a $U_{o,1/3,flood}$ and $U_{o,1/3,ebb}$. The ratio $U_{o,1/3,flood}/U_{o,1/3,ebb}$ ranges between 0.95 and 1.05 for all incident wave angles for 90% of the bursts with $H_{m0}>2$ m(all between −40 and 40°). Only the storms with $H_{m0}>3$ m have $U_{o,1/3,flood}/U_{o,1/3,ebb}\approx$ 0.8–1.05 for an incident wave angle of −40 to 20° (except for one outlier burst which may be a measurement error or due to sensor fouling). This means that the largest waves, which come from the south–west for the observation period, have a larger orbital flow velocity in the direction of wave propagation as expected in shoaling.

The largest wave orbital velocity asymmetry occurred in the same direction as the flood current and could therefore increase the sediment transport rate. The opposite is inferred from the calculations, however. The full signal method yields a smaller net transport rate than the probability method (Table 4) contrary to the expected opposite effect of wave asymmetry. In other words, this effect is negligible.

4.2.4. Comparison with suspended load

Interestingly, Grasmeijer et al. (2005) measured annual suspended loads that are much larger than the bed load measurements presented here. Existing models such as Van Rijn (1984a,b) predicted the suspended load transport rather well but, as shown in this paper, this is not the case for the bed load transports. The Van Rijn models for bed load and suspended load are consistent in the sense that the near-bed reference concentration for suspension is based on the bed load predictor. Consequently, for the present measurement location a suspended to bed load ratio of about unity is expected from the Van Rijn predictors, contrary to the measurements which show a much larger ratio. Also, there are some reports of sediment transport measurements from wave or current bed form migration, of which the rates agree better to existing sediment transport predictors (Kachel and Sternberg, 1971; Nielsen, 1992; Ribberink, 1998; Hoekstra et al., 2004; Holmedal and Myrhaug, 2004). This shows that the present discrepancy between bed load measurements and predictors is not general for coastal areas. We found no explanation for this surprising result, but it may have to do with the fact that the present bed load data were collected in current-only conditions for lack of a method to measure bed load under waves, whereas the suspended load was measured in more energetic conditions (Grasmeijer et al., 2005). Given the lack of bed load measurement methods, we can only speculate whether the Van Rijn, Ribberink or Soulsby and Damgaard models would represent the true bed load transports in storm conditions better than our empirical NS model.

The presence of sand waves in the North Sea demonstrates that bed load must be considerably above incipient motion for a significant part of the year (Passchier and Kleinhans, 2005; Van Dijk and Kleinhans, 2005). The present measurements, on the other hand, demonstrate that in tidal current flow without waves the sediment transport is very small. The solution to this apparent paradox is that the sand waves are formed in stormy conditions when waves stir up sediment and the current transports it.

5. Conclusions

The bed load transport in tidal current conditions on the shoreface and inner shelf off the central Dutch coast is very near incipient motion. Despite the large scatter a trend was observed of measured transports of a factor of 5 smaller than well-known bed load models predict. This is consistent with data-sets from literature of bed load transport very near incipient motion. The factor of 5 is possibly explained by the effect of mud on sediment cohesion and flow turbulence. An empirical North Sea predictor was derived from the data.

Annual transport rates were calculated from empirical probability distributions of near-bed current and orbital velocities. The asymmetry of the tidal current velocity, and therefore the representation of the tidal current climate, has the largest effect on the net transport rate. This emphasizes the need for field measurements of near-bed velocity as well as bed load transport.

The effect of wave stirring increases the flood and ebb transports with a factor of 4 compared to current-only conditions although the net transport does not increase much. The wave height representative of the near-bed orbital flows for purposes of sediment transport calculation is between the H_{rms} and H_{m0} wave heights. The effect of wave orbital asymmetry on sediment transport was negligible.

The largest effect on the gross transport rates is caused by differences between bed load predictors and the empirical bed load predictor derived from the data collected in current-only conditions. The data are in agreement with other data of transport rates very near the beginning of motion.

For 13 m water depth at the Noordwijk field site, the annual flood transport from the new empirical bed load predictor and the observed near-bed current and orbital flow climate is estimated ≈ 2 m^2/year, the annual ebb transport ≈ 1.5 m^2/year and the net transport ≈ 0.5 m^2/year, which is an order of magnitude smaller than earlier estimates by Van Rijn (1997) and Van Rijn et al. (2005a). If an existing bed load predictor is used with the observed flow climate then flood and ebb transports are a factor of two smaller than the earlier estimate and the net transport is a factor of five smaller.

Acknowledgements

We thank the Rijkswaterstaat Directorate North Sea, the Vliestroom and Zirfaea crews for making the offshore Nile

sampler measurements possible. Leo van Rijn, Richard Soulsby, Jan Ribberink, Petra Dankers, Lobke Haaring, Sytze van Heteren and Piet Hoekstra are thanked for the discussion. Jan van de Meene is thanked for providing his data. Three anonymous reviewers are acknowledged for the useful comments that helped to improve the paper. Funded by EC MAST, MAS3-CT97-0086. Please contact MGK to obtain Sandpit papers and the full bed load data set in digital format.

References

Baas, J.H., Best, J.L., 2002. Turbulence modulation in clay-rich sediment-laden flows and some implications for sediment deposition. Journal of Sedimentary Research 72 (3), 336–340.

Emmett, W., 1980. A field calibration of the sediment-trapping characteristics of the Helley–Smith bedload sampler. Geological Survey Professional Paper 1139.

Fernandez Luque, R., Van Beek, R., 1976. Erosion and transport of bed-load sediment. Journal of Hydraulic Research 14 (2), 127–144.

Fredsoe, J., Andersen, K.H., Sumer, B.M., 1999. Wave plus current over a ripple-covered bed. Coastal Engineering 38, 177–221.

Gaweesh, M., van Rijn, L., 1994. Bed-load sampling in sand-bed rivers. Journal of Hydraulic Engineering 120 (12), 1364–1384.

Grasmeijer, B.T., Dolphin, T., Vincent, C., Kleinhans, M., 2005. Suspended sand concentrations and transports in tidal flow with and without waves. In: Van Rijn, L.C., Soulsby, R.L., Hoekstra, P., Davies, A. (Eds.), Sandpit project. Aqua Publications, Amsterdam, The Netherlands, pp. U1–U13.

Hoekstra, P., Bell, P., van Santen, P., Roode, N., Levoy, F., Whitehouse, R., 2004. Bedform migration and bedload transport on an intertidal shoal. Continental Shelf Research 24, 1249–1269.

Holmedal, L.E., Myrhaug, D., 2004. Bed load transport under irregular waves plus current from Monte Carlo simulations of parameterized models with application to ripple migration rates observed in the field. Coastal Engineering 51, 155–172.

Houwman, K.T., Van Rijn, L.C., 2002. Flow resistance in the coastal zone. Coastal Engineering 38, 261–273.

Hubbell, D., 1987. Bed load sampling and analysis. In: Thorne, C., Bathurst, J., Hey, R. (Eds.), Sediment transport in gravel-bed rivers. Gravel Bed Rivers conf. proc., Wiley, London, UK, pp. 89–118.

Kachel, N.B., Sternberg, R.W., 1971. Transport of bedload as ripples during an ebb current. Marine Geology 10, 229–244.

Kemp, P., Simons, R., 1983. The interaction of waves and a turbulent current: waves propagating against the current. Journal of Fluid Mechanics 130, 73–89.

Kleinhans, M.G., Van Rijn, L.C., 2002. Stochastic prediction of sediment transport in sand–gravel bed rivers. Journal of Hydraulic Engineering 128 (4), 412–425.

Kleinhans, M., Montfort, O., Dankers, P., van Rijn, L., Bonne, W., 2005a. Mud dynamics on the shoreface and upper shelf, Noordwijk, The Netherlands. In: Van Rijn, L.C., Soulsby, R.L., Hoekstra, P., Davies, A. (Eds.), Sandpit project. Aqua Publications, Amsterdam, The Netherlands, pp. Q1–Q16.

Kleinhans, M.G., Grasmeijer, B.T., Ruessink, B.G., 2005b. Current roughness over small bedforms and waves. In: Van Rijn, L.C., Soulsby, R.L., Hoekstra, P., Davies, A. (Eds.), Sandpit project. Aqua Publications, Amsterdam, The Netherlands, pp. S1–S10.

Madsen, O.S., Grant, W.D., 1976. Sediment transport in the coastal environment. MIT Ralph M. Parsons Lab. Report, vol. 209. Cambridge, USA.

Meyer-Peter, E., Mueller, R., 1948. Formulas for bed-load transport. Proceedings 2nd meeting. Int. Ass. for Hydraulic Structures Res. Stockholm, Sweden, pp. 39–64.

Mitchener, H., Torfs, H., 1996. Erosion of sand–mud mixtures. Coastal Engineering 29, 1–25.

Nielsen, P., 1992. Coastal bottom boundary layers and sediment transport. No. 4 in Advanced Series on Ocean Engineering. World Scientific, Singapore.

Panagiotopoulos, I., Voulgaris, I., Collins, M.B., 1997. The influence of clay on the threshold of movement of fine sandy beds. Coastal Engineering 32, 19–43.

Parker, G., Klingeman, P., McLean, D., 1982. Bedload and size distribution in paved gravel-bed streams. Journal of Hydraulic Engineering 108 (HY4), 544–571.

Passchier, S., Kleinhans, M.G., 2005. Observations of sand waves, megaripples, and hummocks in the Dutch coastal area and their relation to currents and combined flow conditions. Journal of Geophysical Research 110, F04S15.

Ribberink, J.S., 1998. Bed-load transport for steady flows and unsteady oscillatory flows. Coastal Engineering 34, 59–82.

Shvidchenko, A., Pender, G., Hoey, T., 2001. Critical shear stress for incipient motion of sand–gravel streambeds. Water Resources Research 37, 2273–2283.

Soulsby, R., 1997. Dynamics of marine sands. Thomas Telford Publications, London, UK.

Soulsby, R., Damgaard, J., 2005. Bedload sediment transport in coastal waters. Coastal Engineering 52, 673–689.

Thomas, R., Lewis, J., 1993. A new model for bed load sampler calibration to replace the probability-matching method. Water Resources Research 29 (3), 583–597.

Van de Meene, J.W.H., Van Rijn, L.C., 2000. The shoreface-connected ridges along the central Dutch coast — part 1: field observations. Continental Shelf Research 20, 2295–2323.

Van Dijk, T.A.G.P., Kleinhans, M.G., 2005. Processes controlling the dynamics of compound sand waves in the North Sea, Netherlands. Journal of Geophysical Research 110, F04S10.

Van Rijn, L., 1984a. Sediment transport, part I: bed load transport. Journal of Hydraulic Engineering 110 (10), 1431–1456.

Van Rijn, L., 1984b. Sediment transport, part II: suspended load transport. Journal of Hydraulic Engineering 110 (11), 1613–1641.

Van Rijn, L.C., 1997. Sediment transport and budget of the central coastal zone of Holland. Coastal Engineering 32, 61–90.

Van Rijn, L., Gaweesh, M., 1992. New total sediment-load sampler. Journal of Hydraulic Engineering 112 (12), 1686–1691.

Van Rijn, L.C., Soulsby, R.L., Hoekstra, P., Davies, A., 2005a. Sandpit project. AQUA publications, Amsterdam, The Netherlands.

Van Rijn, L.C., Walstra, D.J.R., Van Kessel, T., 2005b. Net transport rates at the Dutch Noordwijk site, North Sea. In: Van Rijn, L.C., Soulsby, R.L., Hoekstra, P., Davies, A. (Eds.), Sandpit project. Aqua Publications, Amsterdam, The Netherlands, pp. A1–A7.

Wiberg, P., Smith, J., 1989. Model for calculating bed load transport of sediment. Journal of Hydraulic Engineering 115, 101–123.

Wilson, K.C., 1987. Analysis of bed-load motion at high shear stress. Journal of Hydraulic Engineering 115, 97–103.

Zanke, U.C.E., 2003. On the influence of turbulence on the initiation of sediment motion. International Journal of Sediment Research 18 (1), 1–15.